

## Cosmic-Ray Boron Flux Measured from 8.4 GeV/ $n$ to 3.8 TeV/ $n$ with the Calorimetric Electron Telescope on the International Space Station

O. Adriani,<sup>1,2</sup> Y. Akaike,<sup>3,4,\*</sup> K. Asano,<sup>5</sup> Y. Asaoka,<sup>5</sup> E. Berti,<sup>1,2</sup> G. Bigongiari,<sup>6,7</sup> W. R. Binns,<sup>8</sup> M. Bongi,<sup>1,2</sup> P. Brogi,<sup>6,7</sup> A. Bruno,<sup>9</sup> J. H. Buckley,<sup>8</sup> N. Cannady,<sup>10,11,12</sup> G. Castellini,<sup>13</sup> C. Checchia,<sup>6,7</sup> M. L. Cherry,<sup>14</sup> G. Collazuol,<sup>15,16</sup> G. A. de Nolfo,<sup>9</sup> K. Ebisawa,<sup>17</sup> A. W. Ficklin,<sup>14</sup> H. Fuke,<sup>17</sup> S. Gonzi,<sup>1,2</sup> T. G. Guzik,<sup>14</sup> T. Hams,<sup>10</sup> K. Hibino,<sup>18</sup> M. Ichimura,<sup>19</sup> K. Ioka,<sup>20</sup> W. Ishizaki,<sup>5</sup> M. H. Israel,<sup>8</sup> K. Kasahara,<sup>21</sup> J. Kataoka,<sup>22</sup> R. Kataoka,<sup>23</sup> Y. Katayose,<sup>24</sup> C. Kato,<sup>25</sup> N. Kawanaka,<sup>20</sup> Y. Kawakubo,<sup>14</sup> K. Kobayashi,<sup>3,4</sup> K. Kohri,<sup>26</sup> H. S. Krawczynski,<sup>8</sup> J. F. Krizmanic,<sup>11</sup> P. Maestro,<sup>6,7,†</sup> P. S. Marrocchesi,<sup>6,7</sup> A. M. Messineo,<sup>27,7</sup> J. W. Mitchell,<sup>11</sup> S. Miyake,<sup>28</sup> A. A. Moiseev,<sup>29,11,12</sup> M. Mori,<sup>30</sup> N. Mori,<sup>2</sup> H. M. Motz,<sup>31</sup> K. Munakata,<sup>25</sup> S. Nakahira,<sup>17</sup> J. Nishimura,<sup>17</sup> S. Okuno,<sup>18</sup> J. F. Ormes,<sup>32</sup> S. Ozawa,<sup>33</sup> L. Pacini,<sup>1,13,2</sup> P. Papini,<sup>2</sup> B. F. Rauch,<sup>8</sup> S. B. Ricciarini,<sup>13,2</sup> K. Sakai,<sup>10,11,12</sup> T. Sakamoto,<sup>34</sup> M. Sasaki,<sup>29,11,12</sup> Y. Shimizu,<sup>18</sup> A. Shiomi,<sup>35</sup> P. Spillantini,<sup>1</sup> F. Stolzi,<sup>6,7</sup> S. Sugita,<sup>34</sup> A. Sulaj,<sup>6,7</sup> M. Takita,<sup>5</sup> T. Tamura,<sup>18</sup> T. Terasawa,<sup>5</sup> S. Torii,<sup>3</sup> Y. Tsunesada,<sup>36,37</sup> Y. Uchihori,<sup>38</sup> E. Vannuccini,<sup>2</sup> J. P. Wefel,<sup>14</sup> K. Yamaoka,<sup>39</sup> S. Yanagita,<sup>40</sup> A. Yoshida,<sup>34</sup> K. Yoshida,<sup>21</sup> and W. V. Zober<sup>8</sup>

(CALET Collaboration)

<sup>1</sup>*Department of Physics Department of Physics, University of Florence, Via Sansone, 1–50019, Sesto Fiorentino, Italy*

<sup>2</sup>*INFN Sezione di Florence, Via Sansone, 1–50019, Sesto Fiorentino, Italy*

<sup>3</sup>*Waseda Research Institute for Science and Engineering, Waseda University, 17 Kikuicho, Shinjuku, Tokyo 162-0044, Japan*

<sup>4</sup>*JEM Utilization Center, Human Spaceflight Technology Directorate, Japan Aerospace Exploration Agency, 2-1-1 Sengen, Tsukuba, Ibaraki 305-8505, Japan*

<sup>5</sup>*Institute for Cosmic Ray Research, The University of Tokyo, 5-1-5 Kashiwa-no-Ha, Kashiwa, Chiba 277-8582, Japan*

<sup>6</sup>*Department of Physical Sciences, Earth and Environment, University of Siena, via Roma 56, 53100 Siena, Italy*

<sup>7</sup>*INFN Sezione di Pisa, Polo Fibonacci, Largo B. Pontecorvo, 3–56127 Pisa, Italy*

<sup>8</sup>*Department of Physics and McDonnell Center for the Space Sciences, Washington University, One Brookings Drive, St. Louis, Missouri 63130-4899, USA*

<sup>9</sup>*Heliospheric Physics Laboratory, NASA/GSFC, Greenbelt, Maryland 20771, USA*

<sup>10</sup>*Center for Space Sciences and Technology, University of Maryland, Baltimore County, 1000 Hilltop Circle, Baltimore, Maryland 21250, USA*

<sup>11</sup>*Astroparticle Physics Laboratory, NASA/GSFC, Greenbelt, Maryland 20771, USA*

<sup>12</sup>*Center for Research and Exploration in Space Sciences and Technology, NASA/GSFC, Greenbelt, Maryland 20771, USA*

<sup>13</sup>*Institute of Applied Physics (IFAC), National Research Council (CNR), Via Madonna del Piano, 10, 50019 Sesto, Fiorentino, Italy*

<sup>14</sup>*Department of Physics and Astronomy, Louisiana State University, 202 Nicholson Hall, Baton Rouge, Louisiana 70803, USA*

<sup>15</sup>*Department of Physics and Astronomy, University of Padova, Via Marzolo, 8, 35131 Padova, Italy*

<sup>16</sup>*INFN Sezione di Padova, Via Marzolo, 8, 35131 Padova, Italy*

<sup>17</sup>*Institute of Space and Astronautical Science, Japan Aerospace Exploration Agency, 3-1-1 Yoshinodai, Chuo, Sagami, Kanagawa 252-5210, Japan*

<sup>18</sup>*Kanagawa University, 3-27-1 Rokkakubashi, Kanagawa, Yokohama, Kanagawa 221-8686, Japan*

<sup>19</sup>*Faculty of Science and Technology, Graduate School of Science and Technology, Hirosaki University, 3, Bunkyo, Hirosaki, Aomori 036-8561, Japan*

<sup>20</sup>*Yukawa Institute for Theoretical Physics, Kyoto University, Kitashirakawa Oiwakecho, Sakyo, Kyoto 606-8502, Japan*

<sup>21</sup>*Department of Electronic Information Systems, Shibaura Institute of Technology, 307 Fukasaku, Minuma, Saitama 337-8570, Japan*

<sup>22</sup>*Waseda Research Institute for Science and Engineering, Waseda University, 3-4-1 Okubo, Shinjuku, Tokyo 169-8555, Japan*

<sup>23</sup>*National Institute of Polar Research, 10-3, Midori-cho, Tachikawa, Tokyo 190-8518, Japan*

<sup>24</sup>*Faculty of Engineering, Division of Intelligent Systems Engineering, Yokohama National University, 79-5 Tokiwadai, Hodogaya, Yokohama 240-8501, Japan*

<sup>25</sup>*Faculty of Science, Shinshu University, 3-1-1 Asahi, Matsumoto, Nagano 390-8621, Japan*

<sup>26</sup>*Institute of Particle and Nuclear Studies, High Energy Accelerator Research Organization, 1-1 Oho, Tsukuba, Ibaraki 305-0801, Japan*

<sup>27</sup>*University of Pisa, Polo Fibonacci, Largo B. Pontecorvo, 3–56127 Pisa, Italy*

<sup>28</sup>*Department of Electrical and Electronic Systems Engineering, National Institute of Technology, Ibaraki College, 866 Nakane, Hitachinaka, Ibaraki 312-8508 Japan*

<sup>29</sup>*Department of Astronomy, University of Maryland, College Park, Maryland 20742, USA*

<sup>30</sup>*Department of Physical Sciences, College of Science and Engineering, Ritsumeikan University, Shiga 525-8577, Japan*

<sup>31</sup>*Faculty of Science and Engineering, Global Center for Science and Engineering, Waseda University, 3-4-1 Okubo, Shinjuku, Tokyo 169-8555, Japan*

<sup>32</sup>*Department of Physics and Astronomy, University of Denver,**Physics Building, Room 211, 2112 East Wesley Avenue, Denver, Colorado 80208-6900, USA*<sup>33</sup>*Quantum ICT Advanced Development Center, National Institute of Information and Communications Technology, 4-2-1 Nukui-Kitamachi, Koganei, Tokyo 184-8795, Japan*<sup>34</sup>*College of Science and Engineering, Department of Physics and Mathematics, Aoyama Gakuin University, 5-10-1 Fuchinobe, Chuo, Sagami-hara, Kanagawa 252-5258, Japan*<sup>35</sup>*College of Industrial Technology, Nihon University, 1-2-1 Izumi, Narashino, Chiba 275-8575, Japan*<sup>36</sup>*Graduate School of Science, Osaka Metropolitan University, 3-3-138, Sugimoto, Sumiyoshi, Osaka 558-8585, Japan*<sup>37</sup>*Nambu Yoichiro Institute for Theoretical and Experimental Physics, Osaka Metropolitan University, 3-3-138, Sugimoto, Sumiyoshi, Osaka 558-8585, Japan*<sup>38</sup>*National Institutes for Quantum and Radiation Science and Technology, 4-9-1 Anagawa, Inage, Chiba 263-8555, Japan*<sup>39</sup>*Nagoya University, Furo, Chikusa, Nagoya 464-8601, Japan*<sup>40</sup>*College of Science, Ibaraki University, 2-1-1 Bunkyo, Mito, Ibaraki 310-8512, Japan*

(Received 7 October 2022; revised 7 November 2022; accepted 22 November 2022; published 16 December 2022)

We present the measurement of the energy dependence of the boron flux in cosmic rays and its ratio to the carbon flux in an energy interval from 8.4 GeV/ $n$  to 3.8 TeV/ $n$  based on the data collected by the Calorimetric Electron Telescope (CALET) during  $\sim 6.4$  yr of operation on the International Space Station. An update of the energy spectrum of carbon is also presented with an increase in statistics over our previous measurement. The observed boron flux shows a spectral hardening at the same transition energy  $E_0 \sim 200$  GeV/ $n$  of the C spectrum, though B and C fluxes have different energy dependences. The spectral index of the B spectrum is found to be  $\gamma = -3.047 \pm 0.024$  in the interval  $25 < E < 200$  GeV/ $n$ . The B spectrum hardens by  $\Delta\gamma_B = 0.25 \pm 0.12$ , while the best fit value for the spectral variation of C is  $\Delta\gamma_C = 0.19 \pm 0.03$ . The B/C flux ratio is compatible with a hardening of  $0.09 \pm 0.05$ , though a single power-law energy dependence cannot be ruled out given the current statistical uncertainties. A break in the B/C ratio energy dependence would support the recent AMS-02 observations that secondary cosmic rays exhibit a stronger hardening than primary ones. We also perform a fit to the B/C ratio with a leaky-box model of the cosmic-ray propagation in the Galaxy in order to probe a possible residual value  $\lambda_0$  of the mean escape path length  $\lambda$  at high energy. We find that our B/C data are compatible with a nonzero value of  $\lambda_0$ , which can be interpreted as the column density of matter that cosmic rays cross within the acceleration region.

DOI: [10.1103/PhysRevLett.129.251103](https://doi.org/10.1103/PhysRevLett.129.251103)

**Introduction.**—The larger relative abundance of light elements such as Li, Be, and B in cosmic rays (CRs) compared to the Solar System abundance is a proof of their secondary origin. They are produced by the spallation reactions of primary CRs, injected and accelerated in astrophysical sources, with nuclei of the interstellar medium (ISM). Measurements of the secondary-to-primary abundance ratios (as B/C) make it possible to probe galactic propagation models and constrain their parameters, since they are expected to be proportional at high energy to the average amount of material  $\lambda$  traversed by CRs in the Galaxy, which, in turn, is inversely proportional to the CR diffusion coefficient  $D$ . Earlier measurements [1–5] indicate that  $\lambda$  decreases with increasing CR energy per nucleon

$E$ , following a power law  $\lambda \propto E^{-\delta}$ , where  $\delta$  is the diffusion spectral index. The recently observed hardening in the spectrum of CR of different nuclear species [6–12] can be explained as due to subtle effects of CR transport including: an inhomogeneous or an energy-dependent diffusion coefficient [13–15]; the possible reacceleration of secondary particles when they occasionally cross a supernova shock during propagation [16]; and/or the production of a small fraction of secondaries by interactions of primary nuclei with matter (source grammage) inside the acceleration region [17–19]. To investigate these phenomena, a precise determination of the energy dependence of  $\lambda$  is needed. That can be achieved by extending the measurements of secondary CRs in the TeV/ $n$  region with high statistics and reduced systematic uncertainties. In this Letter, we present new direct measurements of the energy spectra of boron, carbon, and the boron-to-carbon ratio in the energy range from 8.4 GeV/ $n$  to 3.8 TeV/ $n$ , based on the data collected by the Calorimetric Electron Telescope (CALET) [20–22] from October 13, 2015, to February 28, 2022, aboard the International Space Station (ISS).

Published by the American Physical Society under the terms of the [Creative Commons Attribution 4.0 International license](https://creativecommons.org/licenses/by/4.0/). Further distribution of this work must maintain attribution to the author(s) and the published article's title, journal citation, and DOI.

*Detector.*—The CALET instrument comprises a charge detector (CHD), a finely segmented preshower imaging calorimeter (IMC), and a total absorption calorimeter (TASC). A complete description of the instrument can be found in Supplemental Material of Ref. [23].

The IMC consists of seven tungsten plates interspaced with eight double layers of scintillating fibers, arranged along orthogonal directions. Fiber signals are used to reconstruct the CR particle trajectory by applying a combinatorial Kalman filter [24]. The estimated error in the determination of the arrival direction of B and C nuclei is  $\sim 0.1^\circ$  with a corresponding spatial resolution of the impact point on the CHD of  $\sim 220 \mu\text{m}$ .

The identification of the particle charge  $Z$  is based on the measurements of the ionization deposits in the CHD and IMC. The CHD, located above the IMC, is comprised of two hodoscopes (CHDX and CHDY) made of 14 plastic scintillator paddles each, arranged perpendicularly to each other. The particle trajectory is used to identify the CHD paddles and IMC fibers traversed by the primary particle and to determine the path length correction to be applied to the signals to extract samples of the ionization energy loss ( $dE/dx$ ). Three charge values ( $Z_{\text{CHDX}}$ ,  $Z_{\text{CHDY}}$ , and  $Z_{\text{IMC}}$ ) are reconstructed, on an event-by-event basis, from the measured  $dE/dx$  in each CHD layer and the average of the  $dE/dx$  samples along the track in the top half of IMC [9]. The CHD can resolve individual chemical elements from  $Z = 1$  to 40, while the saturation of the fiber signals limits the IMC charge measurement to  $Z \lesssim 14$ . The charge resolution of the CHD (IMC) is  $\sim 0.15(0.24)e$  (charge unit) in the elemental range from B to O.

The TASC is a homogeneous calorimeter made of 12 layers of lead-tungstate bars, each read out by photosensors and a front-end electronics spanning a dynamic range  $> 10^6$ . The total thickness of the instrument is equivalent to 30 radiation lengths and 1.3 proton nuclear interaction lengths.

The TASC was calibrated at the CERN Super Proton Synchrotron in 2015 using a beam of accelerated ion fragments with  $A/Z = 2$  and kinetic energy of 13, 19, and 150 GeV/ $n$  [25]. The response curve for interacting particles of each nuclear species is nearly Gaussian at a fixed beam energy. The mean energy released in the TASC is  $\sim 20\%$  of the particle energy, and the resolution is close to 30%. The energy response of the TASC turned out to be linear up to the maximum particle energy (6 TeV) available at the beam, as described in Supplemental Material of Ref. [9].

Monte Carlo (MC) simulations, reproducing the detailed detector configuration and physics processes, as well as detector signals, are based on the EPICS simulation package [26] and employ the hadronic interaction model DPMJET-III [27]. Independent simulations based on GEANT4 10.5 [28] are used to assess the systematic uncertainties.

*Data analysis.*—We have analyzed flight data (FD) collected in 2331 days of CALET operation aboard the ISS. Raw data are corrected for nonuniformity in light output, time and temperature dependence, and gain differences among the channels by using penetrating protons and He particles selected by a dedicated trigger mode [29]. Correction curves for the reduction of the scintillator light yield due to the quenching effect in the CHD and IMC are obtained from FD by fitting subsets for each nuclear species to a function of  $Z^2$  using a “halo” model [30].

Boron and carbon candidates are searched for among events selected by the onboard high-energy (HE) shower trigger, which requires the coincidence of the summed signals of the last two IMC double layers and the top TASC layer. The total observation live time for the HE trigger is  $T = 4.72 \times 10^4$  h, corresponding to 87.2% of the total observation time. In order to mitigate the effect of possible temporal variations of the trigger thresholds on the trigger efficiency, an offline trigger is applied to FD with higher thresholds than the onboard trigger. Triggered particles entering the instrument from lateral sides or late interacting in the lower half of the calorimeter are rejected based on the large fraction of energy leakage estimated from the shape of the longitudinal and lateral shower profiles. All reconstructed events with one well-fitted track passing through the top surface of the CHD and the bottom surface of the TASC (excluding a border region of 2 cm) are then selected. The geometrical acceptance for this category of events is  $S\Omega \sim 510 \text{ cm}^2 \text{ sr}$ .

Boron and carbon candidates are identified by applying window charge cuts of half width  $0.45e$  centered on the nominal values ( $Z = 5, 6$ ) to the distribution of the average charge in the CHD ( $Z_{\text{CHD}}$ ) obtained after requiring that  $Z_{\text{CHDX}}$  and  $Z_{\text{CHDY}}$  are consistent with each other within 10% and  $|Z_{\text{CHD}} - Z_{\text{IMC}}| < 1$ , as shown in Fig. S2 in Supplemental Material [31]. The consistency of the charge values measured by each of the four upper IMC fiber layers is also required.

An additional cut on the track width (TW) is applied to reject particles undergoing a charge-changing nuclear interaction in the upper part of the instrument. The TW variable is defined as the difference, normalized to the particle charge, between the total energy deposited in the clusters of nearby fibers crossed by the reconstructed track and the sum of the fiber signals in the cluster cores. Examples of TW distributions are shown in Fig. S3 in Supplemental Material [31].

The field-of-view (FOV) of CALET at large zenith angle ( $> 45^\circ$ ) is partially shielded by fixed structures on the ISS. Moreover, moving structures (e.g., solar panels and robotic arms) can cross the FOV for short periods of time during ISS operations. CR interactions in these structures can create secondary nuclei that, if detected by CALET, may induce a contamination in the flux measurements. To avoid

that, the events ( $\sim 8\%$  of the final candidate samples) with reconstructed trajectories pointing to obstacles in the FOV are discarded in the analysis.

With this selection procedure,  $1.99 \times 10^5$  B and  $9.27 \times 10^5$  C nuclei are identified. For flux measurements, an iterative unfolding Bayesian method [32] is applied to correct the distributions (Fig. S4 in Supplemental Material [31]) of the total energy deposited in the TASC ( $E_{\text{TASC}}$ ) for significant bin-to-bin migration effects (due to the limited energy resolution) and infer the primary particle energy. The response matrix for the unfolding procedure is derived using MC simulations after applying the same selection procedure as for FD. The energy spectrum is obtained from the unfolded energy distribution as follows:

$$\Phi(E) = \frac{N(E)}{\Delta E \varepsilon(E) S \Omega T}, \quad (1)$$

$$N(E) = U[N_{\text{obs}}(E_{\text{TASC}}) - N_{\text{bg}}(E_{\text{TASC}})] \quad (2)$$

where  $\Delta E$  is the energy bin width;  $E$  the kinetic energy per nucleon calculated as the geometric mean of the lower and upper bounds of the bin;  $N(E)$  the bin content in the unfolded distribution;  $\varepsilon(E)$  the total selection efficiency (Fig. S5 in Supplemental Material [31]);  $U()$  the iterative unfolding procedure;  $N_{\text{obs}}(E_{\text{TASC}})$  the bin content of the observed energy distribution (including background); and  $N_{\text{bg}}(E_{\text{TASC}})$  the bin content of background events in the observed energy distribution. The background contamination in the final B sample is estimated from TW distributions in different intervals of  $E_{\text{TASC}}$ , after applying the complete charge selection procedure. The contamination fraction  $N_{\text{bg}}/N_{\text{obs}}$  is  $\sim 1\%$  for  $E_{\text{TASC}} < 10^2$  GeV and grows logarithmically with  $E_{\text{TASC}}$  for  $E_{\text{TASC}} > 10^2$  GeV, approaching  $\sim 7\%$  at 1.5 TeV. The background is negligible for C.

*Systematic uncertainties.*—Different sources of systematic uncertainties were studied, including trigger efficiency, charge identification, energy scale, unfolding procedure, MC simulations, B isotopic composition, and background subtraction.

The HE trigger efficiency was measured as a function of  $E_{\text{TASC}}$  using a subset of data taken with a minimum bias trigger. The small differences ( $< 1\%$ ) found between the HE efficiency curves and the predictions from MC simulations (Fig. S1 in Supplemental Material [31]) induce a systematic error of  $\pm 0.8\%$  ( $\pm 0.7\%$ ) in the B (C) flux.

The systematic error related to charge identification was studied by varying the width of the window cuts for  $Z_{\text{CHD}}$  between  $0.43e$  and  $0.47e$  and the boundary  $\alpha$  of the consistency cut  $|Z_{\text{CHD}} - Z_{\text{IMC}}| < \alpha$  between 0.9 and 1.1. The result was a flux variation ranging from  $-1.1\%$  to  $3.1\%$  for B and  $-1.5\%$  to  $0.9\%$  for C, depending on the energy bin. The uncertainty ( $\pm 2\%$ ) in the energy scale from the beam test calibration affects the absolute normalization of the B and C spectra by  $\pm 3\%$  but not their shape.

The uncertainty due to the unfolding procedure was evaluated by using different response matrices computed

by varying the spectral index of the generation spectrum of MC simulations. The resulting error in the absolute flux is  $\pm 1.5\%$  for B and  $\pm 0.5\%$  for C.

Since it is not possible to validate MC simulations with beam test data in the high-energy region, a comparison between different MC programs, i.e., EPICS and GEANT4, was performed. We found that the selection efficiencies are similar, but the energy response matrices differ significantly in the low- and high-energy regions. The resulting fluxes for B (C) show discrepancies not exceeding 6% (10%) below 20 GeV/ $n$  and 12% (10%) above 300 GeV/ $n$ , respectively. This is the dominant source of systematic uncertainties.

The uncertainty of the residual background contamination leads to a maximum error of 3% in the B flux above 400 GeV/ $n$  and  $\leq 2\%$  below.

Since CALET cannot distinguish among the B isotopes, the spectral binning in kinetic energy per nucleon is calculated assuming an isotopic composition of 70% of  $^{11}\text{B}$  and 30% of  $^{10}\text{B}$  as in Ref. [6]. We checked with MC that a variation of  $\pm 10\%$  in the abundance of  $^{11}\text{B}$  causes a  $\pm 1\%$  difference in the selection efficiency and a  $\mp 1.7\%$  change in the flux normalization.

Other energy-independent systematic uncertainties affecting the normalization include live time (3.4%, as explained in Supplemental Material of Ref. [23]) and long-term stability of charge calibration (0.5%).

The energy dependence of all the systematic uncertainties is shown in Fig. S6 in Supplemental Material [31]. Finally, an independent analysis, using different tracking and charge identification procedures [33], turned out to be in very good agreement with the results reported in this Letter.

*Results.*—The energy spectra of B and C and their flux ratio measured with CALET are shown in Fig. 1; the corresponding data tables including statistical and systematic errors are reported in Supplemental Material [31]. CALET spectra are compared with results from space-based [1,2,5,7,8] and balloon-borne [3,4,34,35] experiments. The B spectrum is consistent with that of PAMELA [5] and most of the earlier experiments, but the absolute normalization is in tension with that of AMS-02, as already pointed out by our previous measurements of the C, O, and Fe fluxes [9,36]. However, we notice that the B/C ratio [Fig. 1(c)] is consistent with the one measured by AMS-02. The C spectrum shown here is based on a larger dataset, but it is consistent with our earlier result and includes an improved assessment of systematic errors.

Figure 2 shows the fits to CALET B and C data with a double power-law function (DPL)

$$\Phi(E) = \begin{cases} c \left(\frac{E}{\text{GeV}}\right)^\gamma & E \leq E_0, \\ c \left(\frac{E}{\text{GeV}}\right)^\gamma \left(\frac{E}{E_0}\right)^{\Delta\gamma} & E > E_0, \end{cases} \quad (3)$$

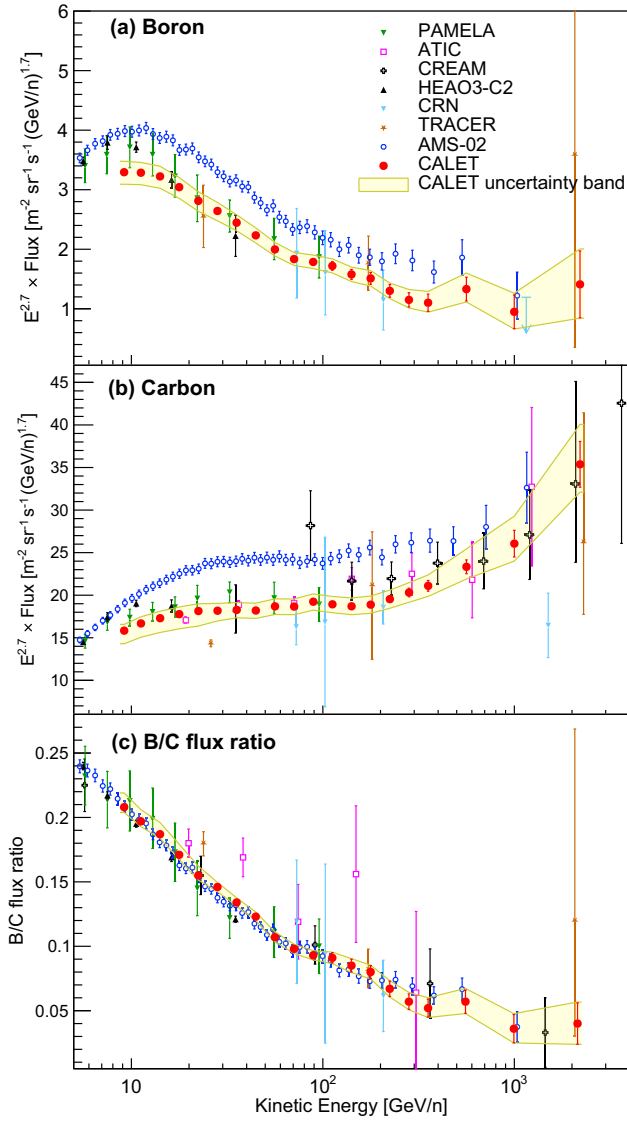


FIG. 1. CALET (a) boron and (b) carbon flux (multiplied by  $E^{2.7}$ ) and (c) ratio of boron to carbon, as a function of kinetic energy per nucleon  $E$ . Error bars of CALET data (red) represent the statistical uncertainty only, while the yellow band indicates the quadratic sum of statistical and systematic errors. Also plotted are other direct measurements [1–5,7,8,34,35]. An enlarged version of the figure is available in Fig. S8 in Supplemental Material [31].

where  $c$  is a normalization factor,  $\gamma$  the spectral index, and  $\Delta\gamma$  the spectral index change above the transition energy  $E_0$ . A single power-law function (SPL) is also shown for comparison, where  $\Delta\gamma = 0$  is fixed in Eq. (3) and the fit is limited to data points with  $25 < E < 200$  GeV/ $n$  and extrapolated above. The DPL fit to the C spectrum in the energy range [25, 3800] GeV/ $n$  yields  $\gamma_C = -2.670 \pm 0.005$  and a spectral index increase  $\Delta\gamma_C = 0.19 \pm 0.03$  at  $E_0^C = (220 \pm 20)$  GeV/ $n$  confirming our first results reported in Ref. [9]. For the B spectrum, the parameter  $E_0^B$  is fixed to the fitted value of  $E_0^C$ . The best fit parameters

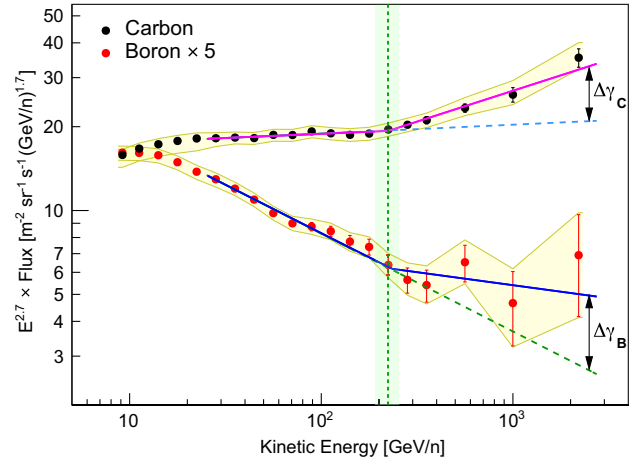


FIG. 2. CALET B (red dots) and C (black dots) energy spectra are fitted with DPL functions (magenta line for C and blue line for B) in the energy range [25, 3800] GeV/ $n$ . The B spectrum is multiplied by a factor 5 to overlap the low-energy region of the C spectrum. The dashed lines represent the extrapolation of a SPL function fitted to data in the energy range [25, 200] GeV/ $n$ .  $\Delta\gamma$  is the change of the spectral index above the transition energy  $E_0^C$  (from the fit to C data), represented by the vertical green dashed line. The green band shows the error interval of  $E_0^C$ .

for B are  $\gamma_B = -3.047 \pm 0.024$  and  $\Delta\gamma_B = 0.25 \pm 0.12$  with  $\chi^2/\text{d.o.f.} = 11.9/12$ . The energy spectra are clearly different as expected for primary and secondary CRs, and the fit results seem to indicate, albeit with low statistical significance, that the flux hardens more for B than for C above 200 GeV/ $n$ . A similar indication also comes from the fit to the B/C flux ratio (Fig. 3). In the energy range [25, 3800] GeV/ $n$ , it can be fitted with a SPL function with spectral index  $\Gamma = -0.366 \pm 0.018$  ( $\chi^2/\text{d.o.f.} = 9.4/13$ ).

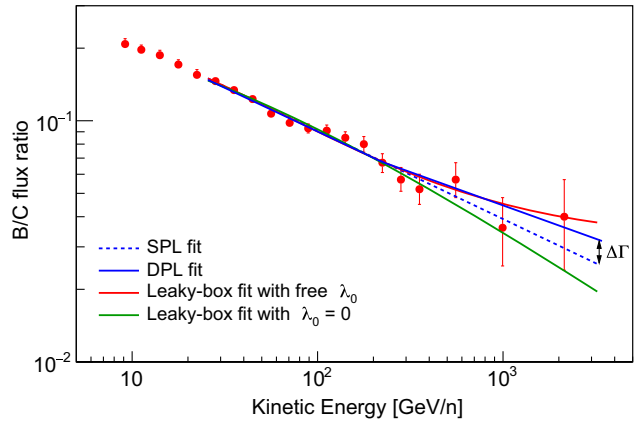


FIG. 3. The CALET B/C ratio fitted to different functions. The error bars are the sum in quadrature of statistical and systematic uncertainties. The data are fitted to a DPL (solid blue line) and a SPL (dashed blue line) function in the energy interval [25, 3800] GeV/ $n$ . The red and green lines represent the fitted functions from a leaky-box model [Eq. (4)] with the  $\lambda_0$  parameter left free to vary and fixed to zero, respectively.

However, a DPL function provides a better fit, suggesting a trend of the data toward a flattening of the B/C ratio at high energy, with a spectral index change  $\Delta\Gamma = 0.09 \pm 0.05$  ( $\chi^2/\text{d.o.f.} = 8.7/12$ ) above  $E_0^C$ , which is left as a fixed parameter in the fit. This result is consistent with that of AMS-02 [7] and supports the hypothesis that secondary B exhibits a stronger hardening than primary C, although no definitive conclusion can be drawn due to the large uncertainty in  $\Delta\Gamma$  given by our present statistics.

Within the “leaky-box” (LB) approximate modeling of the particle transport in the Galaxy [4], the B/C flux ratio can be expressed as

$$\frac{\Phi_B(E)}{\Phi_C(E)} = \frac{\lambda(E)\lambda_B}{\lambda(E) + \lambda_B} \left[ \frac{1}{\lambda_{C \rightarrow B}} + \frac{\Phi_O(E)}{\Phi_C(E)} \frac{1}{\lambda_{O \rightarrow B}} \right], \quad (4)$$

where  $\lambda_B$  is the interaction length of B nuclei with matter of the ISM and  $\lambda_{C \rightarrow B}$  ( $\lambda_{O \rightarrow B}$ ) is the average path length for a nucleus C (O) to spall into B. The spallation path lengths are calculated using the parametrization of the total and partial charge changing cross sections provided in Ref. [37], assuming that they are constant above a few GeV/ $n$ . The  $\Phi_C(E)/\Phi_O(E)$  ratio is measured to be independent of energy and close to 0.91 [9]. The contribution due to the spallation of heavier primary nuclei (Ne, Mg, Si, and Fe) to the B flux is estimated to be  $\sim 10\%$  of the C + O flux, and, therefore, it was not taken into account in Eq. (4). Assuming a composition of the ISM of 90% hydrogen and 10% helium, we calculate  $\lambda_B = 9.4 \text{ g/cm}^2$ , while the constant term enclosed in square brackets in Eq. (4) is  $27 \text{ g/cm}^2$ .

The LB model describes the diffusion of CRs in the Galaxy with a mean escape path length  $\lambda(E)$  which, according to presently available direct measurements, is parametrized as a power-law function of kinetic energy  $E$  as follows:

$$\lambda(E) = kE^{-\delta} + \lambda_0, \quad (5)$$

where  $\delta$  is the diffusion coefficient spectral index. A residual path length  $\lambda_0$  is included in the asymptotic behavior of  $\lambda$ . It can be interpreted as the amount of matter traversed by CRs inside the acceleration region (source grammage). Fitting our B/C data to Eq. (4) (Fig. 3), the best fit values without the source grammage term ( $\lambda_0 = 0$ ) are  $k = 11.2 \pm 0.5 \text{ g/cm}^2$  and  $\delta = 0.52 \pm 0.02$  ( $\chi^2/\text{d.o.f.} = 13.6/13$ ). Leaving instead  $\lambda_0$  free to vary in the LB fit, we obtain  $k = 12.0 \pm 0.9 \text{ g/cm}^2$ ,  $\delta = 0.71 \pm 0.11$ , and  $\lambda_0 = 0.95 \pm 0.35 \text{ g/cm}^2$  ( $\chi^2/\text{d.o.f.} = 9.6/12$ ). These results suggest the possibility of a non-null value of the residual path length (though with a large uncertainty) which could be the cause of the apparent flattening of the B/C ratio at high energy. The best fit values of  $\delta$  and  $\lambda_0$  are compatible with the ones obtained from a combined analysis of the B/C data from earlier

experiments [4] and with the predictions of some recent theoretical works [16,19].

*Conclusion.*—The CR boron spectrum has been measured by CALET up to 3.8 TeV/ $n$  using 76.5 months of data collected aboard the ISS. Our observations show that, despite their different energy dependence, boron and carbon fluxes exhibit a spectral hardening occurring at about the same energy. Within the limitations of our data’s present statistical significance, the boron spectral index change is found to be slightly larger than that of carbon. This trend seems to corroborate the hypothesis that secondary CRs harden more than the primaries, as recently reported by AMS-02 [7]. Interpreting our data with a LB model, we argue that the trend of the energy dependence of the B/C ratio in the TeV/ $n$  region could suggest a possible presence of a residual propagation path length, compatible with the hypothesis that a fraction of secondary B nuclei can be produced near the CR source.

We gratefully acknowledge JAXA’s contributions to the development of CALET and to the operations on board the International Space Station. We also express our sincere gratitude to ASI and NASA for their support of the CALET project. This work was supported in part by JSPS Grant-in-Aid for Scientific Research (S) Grant No. 19H05608, JSPS Grand-in-Aid for Scientific Research (C) No. 21K03592, and the MEXT-Supported Program for the Strategic Research Foundation at Private Universities (20112015) (Grant No. S1101021) at Waseda University. The CALET effort in Italy is supported by ASI under Agreement No. 2013-018-R.0 and its amendments. The CALET effort in the U.S. is supported by NASA through Grants No. 80NSSC20K0397, No. 80NSSC20K0399, and No. NNH18ZDA001N-APRA18-004.

\*yakaike@aoni.waseda.jp

†maestro@unisi.it

- [1] J. J. Engelmann *et al.* (HEAO-3 Collaboration), *Astron. Astrophys.* **233**, 96 (1990).
- [2] S. P. Swordy, D. Mueller, P. Meyer, J. L’Heureux, and J. M. Grunsfeld, *Astrophys. J.* **349**, 625 (1990).
- [3] H. S. Ahn *et al.* (CREAM Collaboration), *Astropart. Phys.* **30**, 133 (2008).
- [4] A. Obermeier, P. Boyle, J. Hörandel, and D. Müller (TRACER Collaboration), *Astrophys. J.* **752**, 69 (2012).
- [5] O. Adriani *et al.* (PAMELA Collaboration), *Astrophys. J.* **93**, 791 (2014).
- [6] M. Aguilar *et al.* (AMS Collaboration), *Phys. Rev. Lett.* **117**, 231102 (2016).
- [7] M. Aguilar *et al.* (AMS Collaboration), *Phys. Rev. Lett.* **120**, 021101 (2018).
- [8] M. Aguilar *et al.* (AMS Collaboration), *Phys. Rep.* **894**, 1 (2021).
- [9] O. Adriani *et al.* (CALET Collaboration), *Phys. Rev. Lett.* **125**, 251102 (2020).

- [10] O. Adriani *et al.* (CALET Collaboration), *Phys. Rev. Lett.* **129**, 101102 (2022).
- [11] Q. An *et al.* (DAMPE Collaboration), *Sci. Adv.* **129**, eaax3793 (2019).
- [12] F. Alemanno *et al.* (DAMPE Collaboration), *Phys. Rev. Lett.* **126**, 201102 (2021).
- [13] G. Jóhannesson *et al.*, *Astrophys. J.* **824**, 16 (2016).
- [14] R. Aloisio, P. Blasi, and P. D. Serpico, *Astron. Astrophys. A* **95**, 583 (2015).
- [15] N. Tomassetti, *Astrophys. J. Lett.* **752**, L13 (2012).
- [16] M. Korsmeier and A. Cuoco, *Phys. Rev. D* **103**, 103016 (2021).
- [17] V. Bresci, E. Amato, P. Blasi, and G. Morlino, *Mon. Not. R. Astron. Soc.* **488**, 2068 (2019).
- [18] R. Cowsik and B. Burch, *Phys. Rev. D* **82**, 023009 (2010).
- [19] C. Evoli, R. Aloisio, and P. Blasi, *Phys. Rev. D* **99**, 103023 (2019).
- [20] S. Torii and P. S. Marrocchesi (CALET Collaboration), *Adv. Space Res.* **64**, 2531 (2019).
- [21] O. Adriani *et al.* (CALET Collaboration), *Phys. Rev. Lett.* **120**, 261102 (2018).
- [22] O. Adriani *et al.* (CALET Collaboration), *Phys. Rev. Lett.* **122**, 181102 (2019).
- [23] O. Adriani *et al.* (CALET Collaboration), *Phys. Rev. Lett.* **119**, 181101 (2017).
- [24] P. Maestro and N. Mori (CALET Collaboration), *Proc. Sci., ICRC2017* (2017) 208, <https://pos.sissa.it/301/208/pdf>.
- [25] Y. Akaike (CALET Collaboration), *Proc. Sci., ICRC2015* (2015) 613, <https://pos.sissa.it/236/613/pdf>.
- [26] K. Kasahara, in *Proceedings of 24th International Cosmic Ray Conference (Rome, Italy)* (1995), Vol. 1, p. 399, <http://cosmos.n.kanagawa-u.ac.jp/EPICSHome/>.
- [27] S. Roesler, R. Engel, and J. Ranft, in *Proceedings of the Monte Carlo Conference, Lisbon, 1033-1038* (Springer, Berlin, Heidelberg, 2000).
- [28] J. Allison *et al.*, *Nucl. Instrum. Methods Phys. Res., Sect. A* **835**, 186 (2016).
- [29] Y. Asaoka *et al.* (CALET Collaboration), *Astropart. Phys.* **100**, 29 (2018); **91**, 1 (2017).
- [30] P. S. Marrocchesi *et al.*, *Nucl. Instrum. Methods Phys. Res., Sect. A* **659**, 477 (2011).
- [31] See Supplemental Material at <http://link.aps.org/supplemental/10.1103/PhysRevLett.129.251103> for supporting figures and the tabulated fluxes, as well as the description of the data analysis procedure and the detailed assessment of systematic uncertainties.
- [32] G. D'Agostini, *Nucl. Instrum. Methods Phys. Res., Sect. A* **362**, 487 (1995); T. Adye, arXiv:1105.1160.
- [33] Y. Akaike and P. Maestro (CALET Collaboration), *Proc. Sci., ICRC2021* (2021) 112, <https://pos.sissa.it/395/112/pdf>.
- [34] A. Panov *et al.* (ATIC Collaboration), *Bull. Russian Acad. Sci.* **73**, 564 (2009).
- [35] H. S. Ahn *et al.* (CREAM Collaboration), *Astrophys. J.* **707**, 593 (2009).
- [36] O. Adriani *et al.* (CALET Collaboration), *Phys. Rev. Lett.* **126**, 241101 (2021).
- [37] W. R. Webber, J. C. Kish, and D. A. Schrier, *Phys. Rev. C* **41**, 520 (1990); **41**, 566 (1990).